Deterministic Frequency-Wavenumber Methods and Direct Measurements of Rupture Propagation During Earthquakes Using a Dense Array: Data Analysis

PETER GOLDSTEIN

Earth Sciences Division, Lawrence Livermore National Laboratory, Livermore, California

RALPH J. ARCHULETA

Department of Geological Sciences, University of California, Santa Barbara

Data recorded by the SMART 1 array in Taiwan are used to make the first direct measurements of two-dimensional earthquake rupture propagation. Using frequency-wavenumber techniques and ray theory, we obtain estimates of the spatial extent, duration, and directions of rupture propagation during two earthquakes located offshore Taiwan. Our estimates include uncertainties due to errors in fault plane location and orientation, velocity structure, and slowness (ray parameter) measured at the array. We find that the January 29, 1981, $M_L = 6.3$ Taiwan earthquake ruptured unilaterally updip and toward the west on a $60°$ dipping, $109°$ striking reverse fault. Using P waves, we find its fault length and duration to be 25 ± 18 km and 7.4 ± 3.4 s, respectively. S waves indicate a fault length and duration of 27 ± 15 km and 9.4 ± 3.6 s, respectively. We suggest that the November 14, 1986, $M_L = 7.0$ Hualien, Taiwan earthquake was triggered by a shallow ($h \approx 14$ km) foreshock $M_L = 5.4$ which occurred on a subparallel or splay fault approximately 5 s before the mainshock. Based on P waves, rupture propagation during the foreshock is unilateral towards the northeast and slightly downdip on a $58°$ dipping, $38°$ striking reverse fault. Its spatial extent and duration are approximately 23 km and 5.4 s. The mainshock initiated at greater depth ($h \approx 34$ km) than the foreshock with its primary direction of rupture unilateral toward the northeast and slightly updip on a $57°$ dipping, $43°$ striking reverse fault. Using P waves, we found a spatial extent and duration of 68 ± 15 km and 12.4 ± 2.2 s. S waves indicate a similar extent, duration, and direction of propagation for the mainshock. However, we found it difficult to distinguish the foreshock and mainshock S waves. We show, by example, that these results represent an improvement over what can be obtained using long-period (T > 5 s) teleseismic methods. Comparison of our results with those obtained using teleseismic data suggests either a short duration slip-time function or that most slip occurs near the rupture front. Our results indicate that much of the complexity in the seismograms recorded during these events, by the SMART 1 array, is due to spatial and temporal variations of the source. This suggests that, at least in some cases, predictions of both the phase and amplitude of strong ground motion, as a function of time, would require a priori knowledge of source properties. Finally, we recommend siting small (≈ 10 station) dense arrays on land above offshore subduction zones, which are considered seismic gaps, because they can provide more detailed measurements of rupture propagation than is presently possible.

INTRODUCTION

In this paper we use array analysis methods developed in an accompanying paper [*Goldstein and Archuleta*, this issue; hereafter Paper 1] to measure two-dimensional, time-dependent, earthquake rupture properties. Unlike most previous measurements of rupture propagation, we include estimates of errors which take into account the uncertainties in our models of velocity structure and fault plane parameters as well as limitations of the data. Such measurements are important because they provide guidelines for differentiating between plausible and unrealistic earthquake source models. They may also

be useful for the prediction of strong ground motion and for studies involving earthquake prediction.

Until recently, most measurements of earthquake source properties have been limited to teleseismic studies where spatial and temporal resolution are limited [e.g., *Gutenberg*, 1955; *Ben-Menahem and Toksoz*, 1962; *Press et al.*, 1961; *Benioff et al.*, 1961; *Kikuchi and Fukao*, 1985], forward modeling where solutions may be highly nonunique [e.g., *Hartzell and Helmberger*, 1982; *Archuleta*, 1984], and inverse modeling where a final model may be sensitive to the initial starting model and trade-offs exist between model variance and spatial resolution [e.g., *Olson and Apsel*, 1982; *Hartzell and Heaton*, 1983; *Olson and Anderson*, 1988; and *Beroza and Spudich*, 1988].

An alternative approach is to measure time-dependent changes in signal properties of an earthquake, at a dense array, and relate these changes to the

earthquake's rupture properties. An important advantage of such measurements is that there is limited risk of relating a peak in one seismogram with an unrelated peak in another. Such measurements are not restricted to long periods and are referred to as direct measurements, because they do not require assumptions about the spatial extent of the source or its rupture time history and they make a direct correspondence between changes in signal properties and the spatio-temporal evolution of the source. For example, Niazi [1982] used temporal changes in horizontal component particle motions recorded at the El Centro differential array to observe northwestward rupture propagation, with rupture velocity ranging between 2.0 and 3.0 km/s, during the 1979 Imperial Valley earthquake. Spudich and Cranswick [1984] used temporal changes in horizontal phase velocity observed at the El Centro differential array to estimate this event's direction (northwestward) and velocity (variable, $\approx$2.8 km/s, and briefly supershear) of rupture propagation. Unfortunately, in both of these studies it was necessary to assume a constant source depth (an assumption that can lead to inaccurate estimates of rupture velocities) and that a single signal was being observed during each measurement interval (an unlikely occurence in the near source region of an earthquake). We solve these problems by using frequency-wavenumber techniques with two-dimensional arrays, because they are not restricted to the observation of a single signal and provide more precise estimates of a signal's direction of arrival than polarization methods [e.g., Harris, 1990].

In this paper we use the techniques described in Paper 1 and data recorded by the SMART 1 array in Taiwan to determine rupture properties of two earthquakes located offshore northeastern Taiwan. We begin by studying the January 29, 1981, M_L = 6.3 Taiwan earthquake. Previous attempts to study rupture propagation during this event, using data recorded at the SMART 1 array, have met with limited success. Examples include Bolt et al. [1982a], who tried to estimate this event's direction of propagation using time dependent, signal azimuths but obtained inconsistent results from P and S waves. Abrahamson [1985] also used time dependent, signal azimuths but had to assume a rupture direction to estimate this event's speed of rupture propagation and only estimated it during the first few seconds of the S waves. In a related study, Darragh [1987] observed changes in source azimuth that were in the opposite direction to that obtained by Abrahamson [1985] but did not attempt to estimate this event's rupture properties. Goldstein [1988] obtained fairly consistent P and S wave estimates of this event's direction of propagation but noted that his estimates of fault length were too large. We improve upon these studies by obtaining consistent P and S wave estimates of this event's spatial extent, duration, and direction of rupture propagation that include uncertainties due to limitations of the

data and our knowledge of the velocity structure and source parameters. We also study rupture propagation during the November 14, 1986, M_L = 7.0 Hualien, Taiwan earthquake and its foreshock M_L = 5.4. We compare our results to those obtained by Hwang and Kanamori [1989], who used the method of Kikuchi and Fukao [1985], to show that our approach has better resolution than long-period ($T > 1$ s) teleseismic methods. Based on a comparison of the long-period, teleseismic and high-frequency, strong ground motion estimates of duration, we suggest that most of the slip is of short duration in comparison to that which would be expected from source size scaling relations (e.g., T. H. Heaton, unpublished manuscript, 1990).

THE SMART 1 ARRAY

Data used in this study were recorded by the SMART 1 strong motion array in Taiwan [Bolt et al., 1982b]. Abrahamson et al. [1987] provide an excellent review of the engineering research that has been done using data from this array, as well as, its instrumentation, site geology, and the regional seismicity and tectonics. Here we give a brief description of the SMART 1 array which is located in the northeastern corner of Taiwan, near the town of Lotung, north of the convergence of the Philippine Sea and Eurasian plates. This digital, strong motion array consists of 36 accelerometers in three concentric rings, two stations to the south of the main array, and one central station (see Figure 1). The three main rings, called inner (I), middle (M), and outer (O), have radii of 200 m, 1 km, and 2 km, respectively. The stations to the south of the main array (E01 and E02) are located 2.8 and 4.8 km from
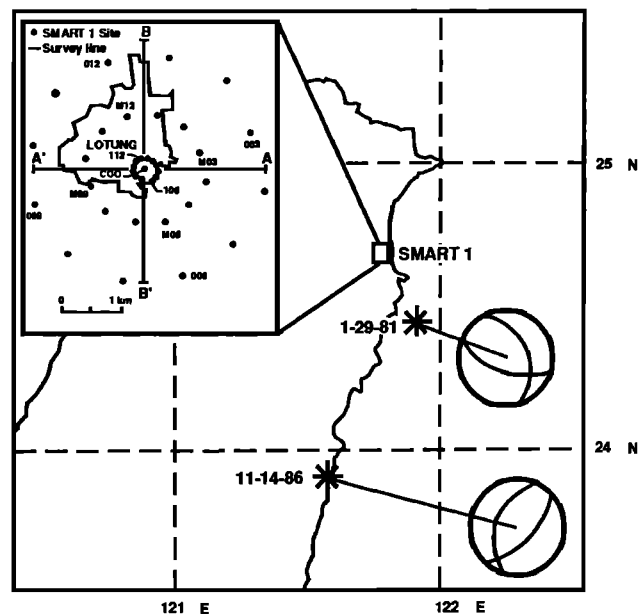

Fig. 1. Locations and focal mechanisms of the January 29, 1981, and November 14, 1986, Taiwan earthquakes. The SMART 1 array is shown as an inset.
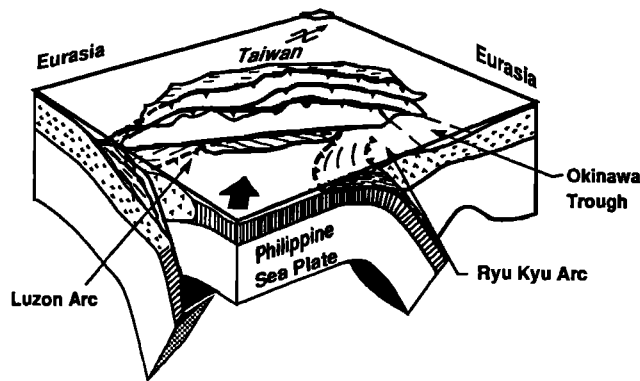
Fig. 2. Lithospheric structure in the vicinity of Taiwan [after *Angelier*, 1986].

the central station. All the stations in the array are sited in an alluvial valley except for E02 which resides on a slate outcrop. Fortuitously, the array contains six linear, equally spaced subarrays (Figure 1) which are necessary for subarray spatial averaging.

Since its installation in 1980, the SMART 1 array has recorded more than 50 shallow to intermediate depth earthquakes with local magnitudes greater than 4.0 and epicentral distances less than 100 km. This high rate of seismicity is a consequence of the complex tectonics of the region surrounding Taiwan (Figure 2) and has provided us with an excellent data set for studying rupture propagation during earthquakes.

JANUARY 29, 1981, TAIWAN EARTHQUAKE

The January 29, 1981 (M_L=6.3) Taiwan earthquake has received considerable attention [see *Abrahamson et al.*, 1987 for references] because it was the only earthquake which produced large accelerations (> 0.25 g) and triggered all the instruments of the SMART 1 array during its first 5 years of operation. Our preferred hypocentral location, discussed later, is 24.49°N, 121.88°E, h=38 km (from the bulletin of the International Seismological Center (ISC) in Newbury, England). *Abrahamson* [1985] determined this event's focal mechanism and noted that the aftershock distribution suggested unilateral rupture towards the west on a fault plane with strike 109 ± 8°, dip 61 ± 5°, and rake 64 ± 4°.

Vertical and north-south component accelerations from five stations forming an approximately linear, equally spaced, subarray running from north to south are shown in Figure 3. Vertical traces have been low-pass filtered at 5 Hz so that waveform correlations are visible. Although a number of pulses can be followed by eye from trace to trace, it is usually difficult to estimate arrival times of specific pulses at all the stations in the array because of interference from other arrivals. Exceptions are the early arriving P wave pulse and the large broad S wave pulse observed at around 3.5 and 8.5 s on the vertical and horizontal components, respectively, of station c00. Following

Goldstein [1988], we used these pulses as our reference pulses for seismogram alignment and estimated their azimuths and angles of incidence using a least squares, plane wave fit to their time delays. Azimuths of the P and S wave pulses were 118 ± 6° and 112 ± 6°, respectively. In contrast, the expected source azimuth is around 150° suggesting strong lateral refractions or inaccurate hypocentral locations. Our analysis suggests a combination of both.

We used MUSIC with seismogram alignment, sub-array spatial averaging, and slowness stacking to calculate frequency-slowness spectra during consecutive, 1.28 s long, 0.5 s overlapping windows beginning at 2.0 s into the record at station c00 for P waves and 7.0 s for S waves (Figure 3). We continued processing the data during successive windows until there was no evidence of arrivals with slownesses corresponding to body waves from the source region. We used vertical components to study the P waves and both horizontals to study the S waves. The cross-spectral matrix was averaged over submatrices corresponding to linear, equally spaced subarrays using subarray spatial averaging. Frequency-slowness spectra were slowness-stacked over ten frequencies from 2.0 to 10.0 Hz. Eight P wave and four S wave frequency-slowness spectra had peak amplitudes more than 1 dB above the background level (dbab), defined to be two standard deviations above the mean power spectral level (Figure 4). To avoid bias in our estimates of the mean and standard deviation of the power spectral level, due to signal peaks, we re-computed the mean and standard deviation five times. Each time we removed points more than two standard deviations above the previous estimate's mean. Based on simulations and experience with data, we found that this procedure usually removes most but not all of the signal's contribution to the mean and standard deviation. However, if no signal is present this procedure will slightly underestimate the mean and standard deviation, emphasizing small spurious peaks. We avoid confusing these peaks with signals by restricting our analysis to spectra with peaks more than 1 dB above the background level.

Our velocity model (Figure 5) consists of a set of gradients over a halfspace. Surface velocities are constrained by the results of *Wen and Yeh* [1984], who performed a refraction survey to determine the velocity structure directly beneath the SMART 1 array. From about 1 to 10 km we approximate the model obtained by *Roecker et al.* [1987], who simultaneously inverted P and S wave travel times of more than 1200 Taiwan earthquakes for their hypocentral locations and the velocity structure beneath Taiwan. Below 10 km we approximate the model obtained by *Hagen et al.* [1988], who used trial and error forward modeling of refraction data from three, ocean bottom seismometers to determine the velocity structure offshore eastern Taiwan. We assumed a constant P to S wave velocity ratio of 1.78 to determine the S wave velocity structure.
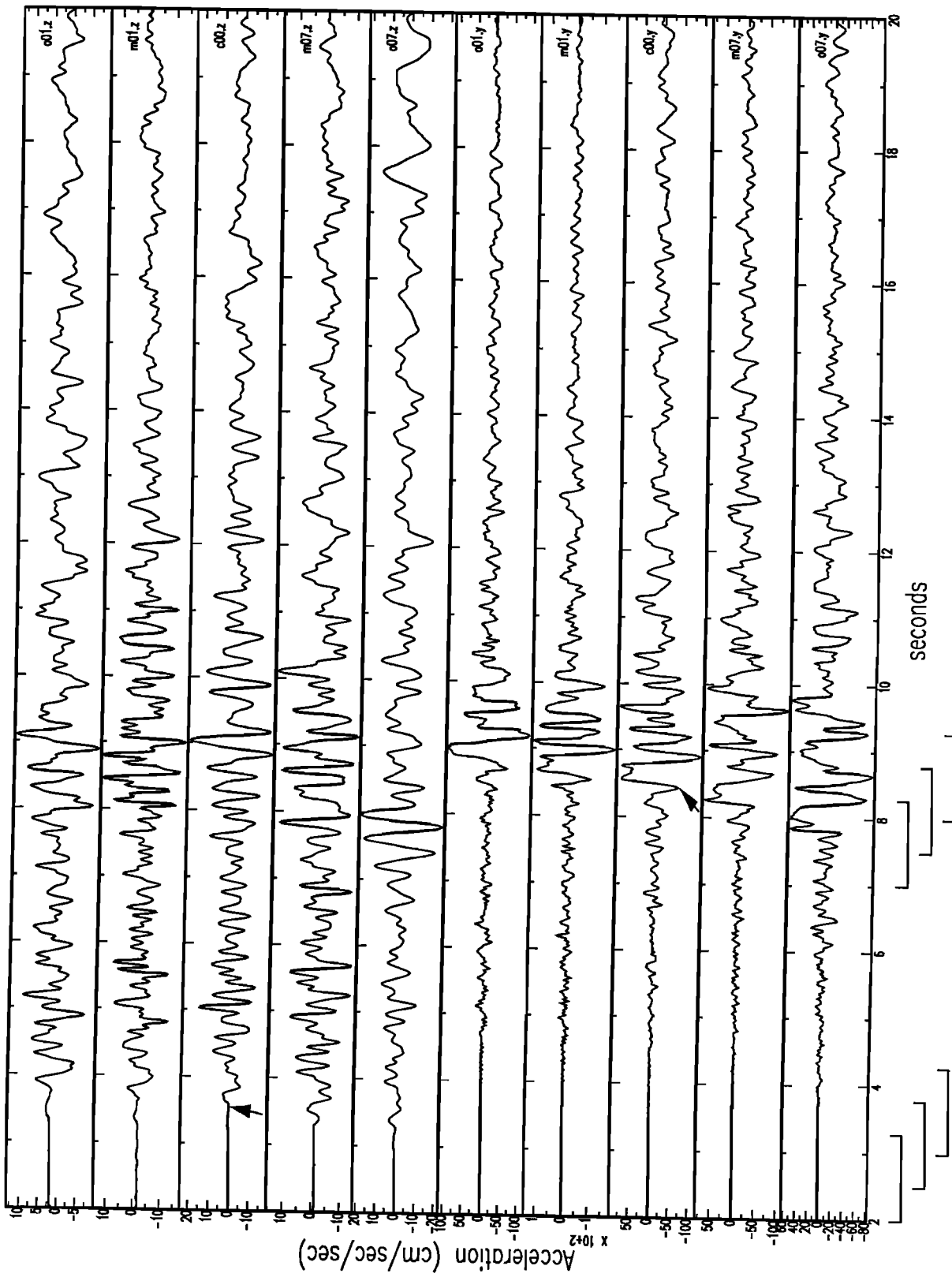
Fig. 3. Vertical and north-south traces recorded at a linear, equally spaced subarray of the SMART 1 array during the January 29, 1981, Taiwan earthquake. Reference phases used to align the traces are indicated by the arrows. Analysis windows are shown at bottom.
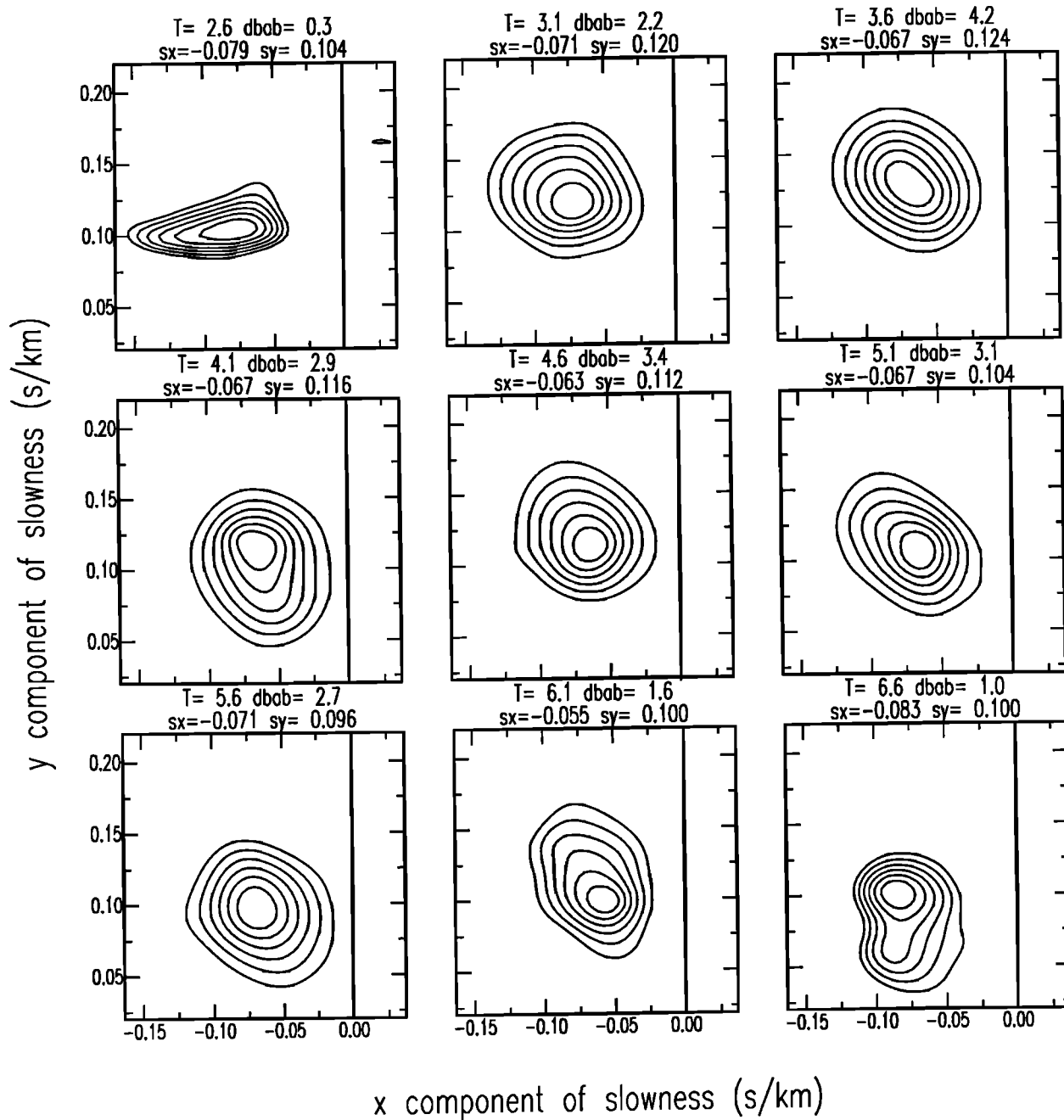
Fig. 4. P wave frequency-slowness spectra from successive windows of the January 29, 1981, Taiwan earthquake. The center time of each window is indicated at the top of each spectrum; dbab indicates the height of the peak in decibels above our baseline, defined as two standard deviations above that plots average power spectral level.

We determine time varying, source locations by projecting our frequency-slowness spectra down onto a fault plane (Figure 6). Our preferred hypocentral location and fault plane parameters are listed above. Before projecting our spectra down onto the fault, we shifted all the P and S wave slownesses so that the earliest arriving P and S waves were coming from a common hypocenter in the preferred model. Although this was not essential to our analysis, it made it much easier to compare P and S wave results. P and S wave source locations, including error bars and labeled by rupture times, are shown as a sequence of snapshots of

the fault plane in Figures 7 and 8, respectively. Small differences in P and S wave hypocentral locations are the result of averaging over a range of plausible fault and velocity models. The approximate time at which each source's signal is observed at the array, relative to the start time of the seismogram, is shown at the top of each plot. Both P and S wave source locations and rupture times clearly indicate a progression from the downdip southeastern end of the fault toward the updip northwestern end of the fault.

Potential sources for errors in our source locations and rupture times include uncertainties in hypocentral
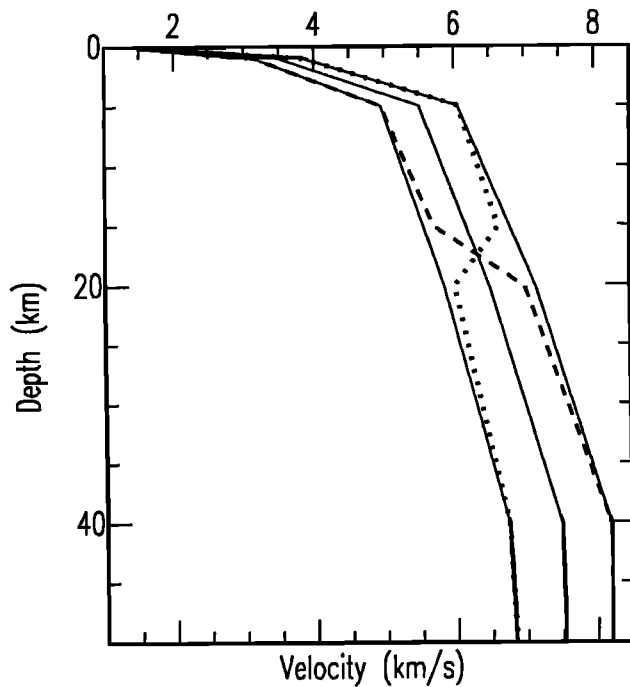
Fig. 5. Five of the velocity models used to project frequency-slowness spectra down onto the fault plane. The central, solid line is our preferred model. The other solid lines indicate our systematically fast and slow models. The dashed lines indicate models which started out too slow and then were too fast, and vice versa.

location, focal mechanism, velocity structure, and slowness estimates. We estimate the size of these errors by combining errors due to uncertainties in slowness with errors estimated from models with a range of source parameters and velocity structures. Models that gave unrealistic rupture properties, such as, fault length and duration much larger or smaller than would be expected for an earthquake of this magnitude, or
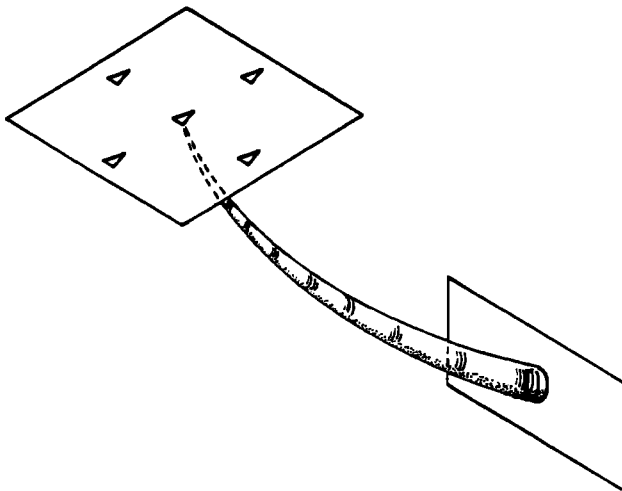
Fig. 6. Schematic illustration of the effect of uncertainties in slowness on our source locations. A cone of rays defined by uncertainties in slowness spreads out as it propagates through the velocity structure. The intersection of this cone with the fault is an ellipse indicating the uncertainty in location.
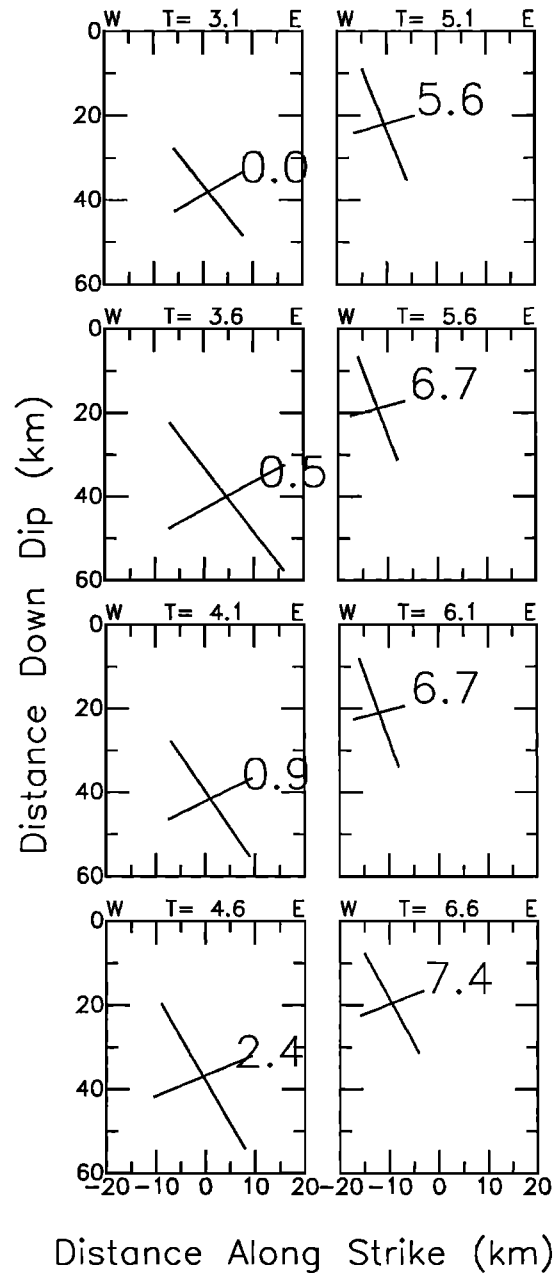
Fig. 7. Snapshots of the January 29, 1981, Taiwan earthquake's fault plane indicating P wave source locations, including error bars and labeled by rupture times. Uncertainties in rupture times are roughly 3.5 s. Each snapshot corresponds to a 1.28-s-long time window at the array. The center time of each window is given at the top of each snapshot.

inconsistent P and S wave estimates for the directions of rupture propagation, were not used to estimate errors.

We began by varying the hypocentral location because there are large variations in those reported by different organizations to the ISC. We prefer the location obtained by the ISC because it is the only one which gave realistic rupture properties. We added small perturbations (<4 km) to the ISC location and found that source locations and rupture times were most sensitive to perturbations in the direction of the
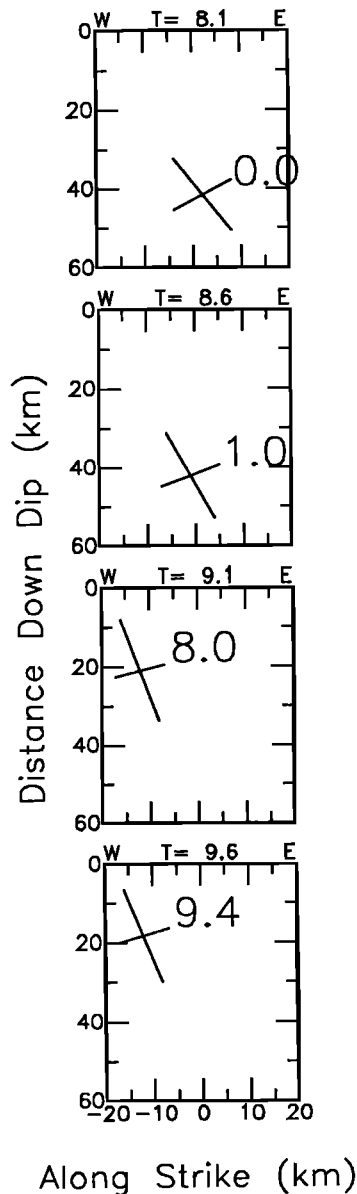
Fig. 8.   Snapshots of the January 29, 1981, Taiwan earthquake's fault plane indicating S wave source locations, including error bars and labeled by rupture times. Uncertainties in rupture times are roughly 3.5 s. See Figure 7.

fault normal. In fact, perturbations greater than 2 km toward the southwest produced unrealistic rupture properties. We varied the strike and dip by ±5° and ±10° and found that variations were moderate to small except when the strike was reduced by 10° or the dip was increased. We also tried using the fault plane conjugate to our preferred solution and found that it gave unrealistic rupture properties. We modeled uncertainties in velocity structure using the velocity models shown in Figure 5 and found that localized variations in the velocity structure were insignificant. However, systematically mismodeling the velocity structure did produce significant variations, especially for deeper sources. Using the formula developed in Paper 1, we estimated two standard

deviations in slowness to be about 0.004 s/km. This uncertainty in slowness defines a cone of rays whose intersection with the fault plane indicates a range of possible source locations (Figure 6). We found that the deeper more distant sources have the largest uncertainties, approximately 15 km, because the cone of rays spreads out as it travels down through the Earth. As a first approximation, we assume model errors and slowness errors are independent and estimate the total error in location and rupture time to be roughly 18 km and 3.4 s for P waves and 15 km and 3.6 s for S waves.

Our P and S wave source locations were used to make separate estimates of the spatial extent, duration, and directions of rupture propagation. P wave source locations and rupture times indicate a fault length and duration of 25 ± 18 km and 7.4 ± 3.4 s, respectively. S wave locations and rupture times indicate a fault length and duration of 27 ± 15 km and 9.4 ± 3.6 s, respectively. Both P and S wave locations indicate that rupture progressed unilaterally updip and toward the west. Rupture velocities are very poorly constrained. Additional discussion of these results is presented in a later section.

NOVEMBER 14, 1986, TAIWAN EARTHQUAKE

The November 14, 1986 (M_L = 7.0) Hualien, Taiwan earthquake is the largest event recorded by the SMART 1 array. This event was responsible for considerable damage and injury in northern Taiwan, and was felt throughout Taiwan and many of the surrounding islands. As we observed with the previous event, there are wide variations (greater than 30 km) between reported hypocentral locations. We prefer the location given by the National Earthquake Information Center (NEIC), Boulder, Colorado, because they were the only organization to note the small foreshock, consistent with our observations, about 5 s before the mainshock. Their origin times and locations are also more consistent with ours than those obtained by other organizations (Regional catalogue of earthquakes, ISC). Our preferred hypocentral parameters for the foreshock and the mainshock are 23.9°N, 121.7°E, h=14.0 km and 23.901°N, 121.575°E, h=34 km, respectively. The above depth for the foreshock is a guess based on our projected source locations and the location of the mainshock obtained by the local network which we suspect is closer to the foreshock location. Using teleseismic P waves, NEIC obtained a mainshock fault plane solution (NP1) with strike (ϕ) = 38°, dip (δ) = 58°, and rake (λ) = 85° or (NP2) with ϕ = 227°, δ = 32°, and λ = 98° (Figure 1). Chen and Wang [1988] noted that data from the Taiwan Telemetered Seismic Network show two impulsive P waves with the same polarities on all the stations and inferred a similar focal mechanism for both the foreshock and the mainshock. They also studied aftershocks and focal mechanisms during the two weeks following this event and found that they support the NP1 fault plane

which is consistent with the compressional tectonics and geology of this area. To test this choice, we tried using the conjugate fault and found plausible but less realistic results than those obtained using NP1. Using Love and Rayleigh waves recorded at stations in the Global Digital Seismic Network, *Hwang and Kanamori* [1989] claim "a more robust determination of the focal mechanism" is strike $(\phi) = 43°$, dip $(\delta) = 57°$, and rake $(\lambda) = 100°$. We use this solution to describe the mainshock fault plane and the first motion solution to describe the foreshock.

Vertical and horizontal component seismograms from a linear subarray trending from north to south are shown in Figure 9. Vertical components have been low-passed filtered at 5 Hz so that waveform correlations are visible. As we found with the previous event, there are a number of pulses that can be correlated by eye but cannot be used as a reference pulse because of interference. Fortunately, the P wave pulse which arrives around 5.5 s into the record at c00 was clearly visible at all the stations in the array. Based on its timing and the sudden change in signal amplitudes this pulse appears to be the first arrival from the mainshock. We used this pulse's time delays between stations to align our P waves. The best least squares, plane wave fit to these time delays gave an azimuth of $183\pm2°$. The difference between our azimuth estimate and that of our preferred hypocentral location ($192°$) is in a direction consistent with the difference found for the other events we studied. We tried to align our S waves using some of the larger pulses that arrive during the S wave window but found many stations with problematic interference effects. Instead, we computed S wave time delays in terms of P wave time delays assuming a constant P to S wave velocity ratio of 1.78.

We computed frequency-slowness spectra for consecutive, overlapping P and S wave windows begining at 2.0 and 10.0 s, respectively. Each window was 1.28 s long with 0.5 s offset from the start of one window to the start of the next (Figure 9). P and S wave spectra were calculated using verticals and horizontals, respectively. We smoothed cross spectral matrices using subarray spatial averaging and six, linear, equally spaced subarrays (Figure 1). We slowness stacked our spectra over five frequencies ranging between 2.0 and 6.0 Hz. Twenty P and 18 S wave spectra had significant signal-to-noise ratios (dbab > 1.0) and were used to determine time dependent source locations.

Time dependent source locations were obtained by projecting frequency-slowness spectra onto a fault plane in the velocity structure described earlier (Figure 5). We found foreshock locations and rupture times using P wave spectra of time windows before the sudden change in P wave amplitudes approximately 5.5 s into the record of station c00. The remaining P wave spectra were projected onto the mainshock fault plane. Foreshock and mainshock source locations, including error bars and labeled by rupture times, are shown as

a sequence of snapshots of the fault plane in Figures 10 and 11. P wave source locations and rupture times of the foreshock (Figure 10) indicate unilateral rupture propagation from the southwest toward the northeast and downdip. P wave source locations and rupture times for mainshock (Figure 11) indicate rupture propagation slightly updip and towards the northeast. S wave, source locations and rupture times are in good agreement with mainshock, P wave results. Unfortunately, we were unable to make a clear distinction between the foreshock and mainshock S waves.

We estimated errors in source locations and rupture times by combining errors based on uncertainties in slowness with errors based on perturbations to our velocity structure (Figure 5), preferred hypocentral locations ($\Delta x \leq 5$ km), and fault plane solutions ($\Delta\phi$ and $\Delta\delta \leq 10°$). Based on two standard deviations in slowness and results from our range of source parameters, errors in P wave source locations and rupture times are 15 km and 2.2 s.

P wave source locations and rupture times indicate a foreshock fault length and duration of 23 ± 12 km and 5.4 ± 2.2 s. The mainshock fault length and duration are 68 ± 15 km and 12.4 ± 2.2 s. Again, rupture velocities are poorly constrained.

DISCUSSION

In previous sections we described direct measurements of two-dimensional rupture propagation during earthquakes. Here, we compare our results with previous observations and discuss them in terms of current hypotheses regarding earthquake sources. We also discuss advantages and limitations of our approach.

We begin by comparing our results for the November 14, 1986, Hualien, Taiwan earthquake with those obtained by *Hwang and Kanamori* [1989], who used long-period, teleseismic P waves, and the method of *Kikuchi and Fukao* [1985]. We note that the long-period, teleseismic source-time function obtained by Hwang and Kanamori (Figure 12) suggests that most of the moment release occurred in approximately 15 s. This is in excellent agreement with the duration we observed (≈12.5 s, Figure 11) and suggests that the duration of most of the slip was short. This lends some support to the recent suggestion by T. H. Heaton (unpublished manuscript, 1990) that earthquakes propagate as short duration pulses of slip. The small pulses that occur later in their teleseismic source-time function might correspond to a small amount of additional slip. However, based on the periodic appearance of the teleseismic source-time function it seems more likely that they are multiples unaccounted for by the velocity model.

In contrast to the duration, there are notable differences in the teleseismic and strong motion estimates of spatial extent and directions of propagation. We ob-
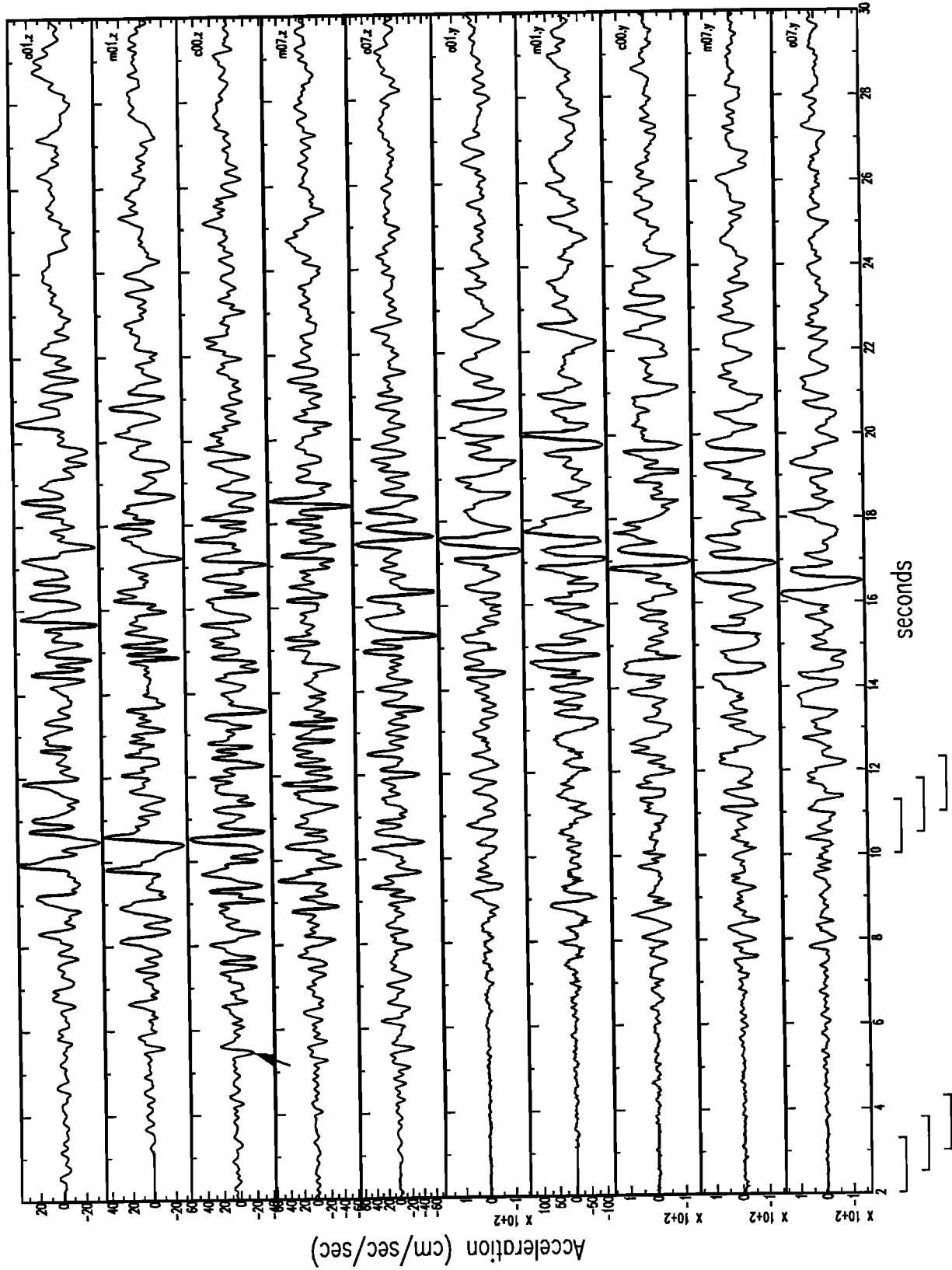
Fig. 9. Vertical and north-south traces recorded at a linear subarray of the SMART 1 array during the November 14, 1986, Hualien, Taiwan earthquake. See Figure 3 and text.
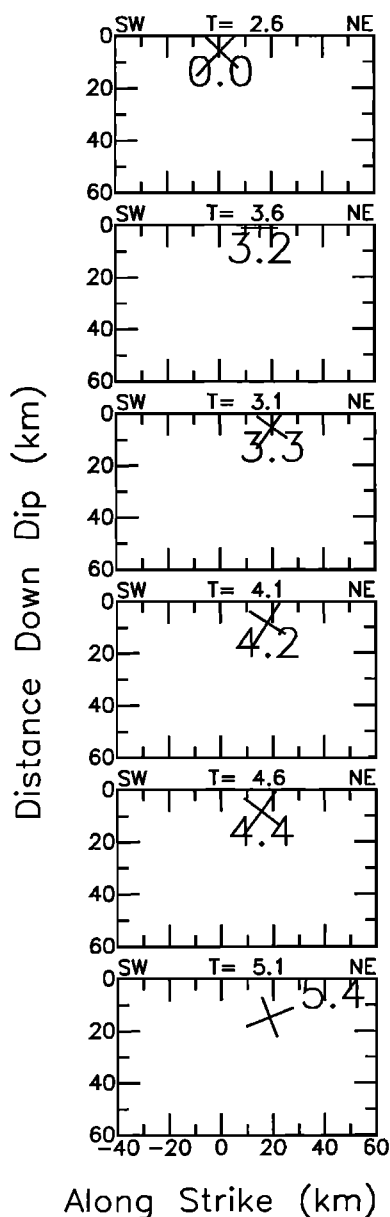
Fig. 10. Snapshots of the November 14, 1986, Hualien, Taiwan earthquake's foreshock fault plane indicating P wave source locations, including error bars and labeled by rupture times. Uncertainties in rupture times are roughly 2.0 s. See Figure 7.

have obtained better resolution of this event's subevents or asperities than the teleseismic study of Hwang and Kanamori. In particular, we have resolved the foreshock as well as the mainshock direction and extent of propagation without constraining the spatial extent of faulting or the velocity of propagation. Furthermore, we obtained consistent results using S waves and our results include estimates of uncertainties. Hwang and Kanamori did obtain additional locations but found that only the first five were insensitive to the model parameters (L.J. Hwang, private communication, 1990).

It is interesting to compare our observation of rupture propagation with current hypotheses that relate directions of propagation to seismicity and depth. For example, our finding that rupture propagated from the hypocenter of the January 29, 1981, Taiwan earthquake toward the main concentration of aftershock locations obtained by Abrahamson [1985] is consistent with many previous observations that aftershocks tend to concentrate in regions where the rupture terminates [e.g., Benioff, 1955; Mendoza and Hartzell, 1988]. However, seismicity following the November 14, 1986,

serve primarily unilateral progression of the source from the southwest towards the northeast and slightly updip over a distance of about 70 km. The teleseismic estimates suggest bilateral propagation along a more vertical trend and an extent of approximately 40 km. One might argue that the differences indicate that the long-period and high-frequency waves are generated at different places and times. While this may be true in part, it would require a rather complicated spatial variation of the slip-time function. A more plausible explanation is that differences are due to uncertainties in both the teleseismic and strong motion results.

Based on the number of sources, their separations, and rupture times (Figures 10, 11, and 12), we claim to
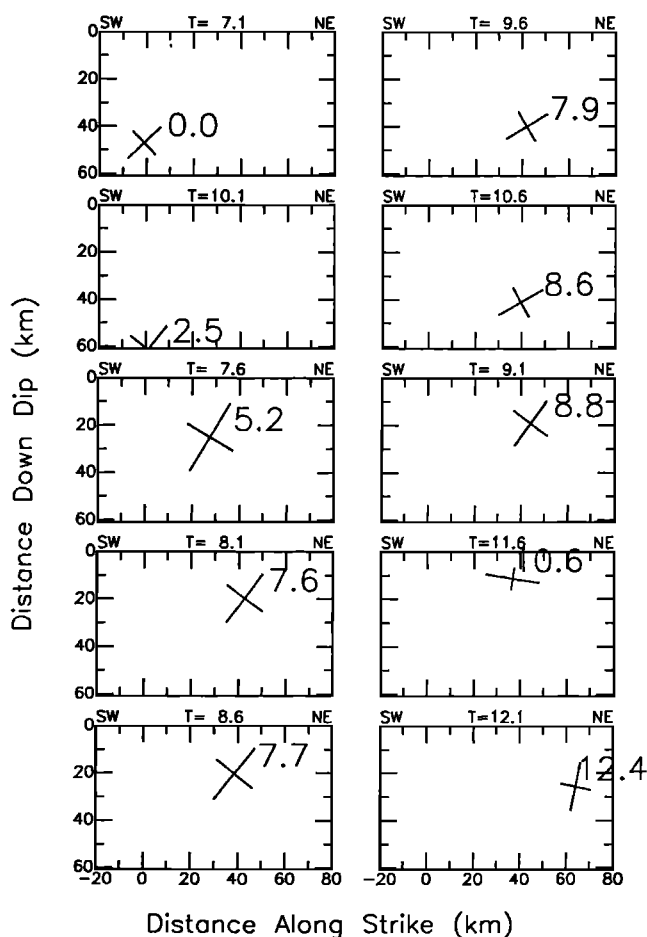
Fig. 11. Snapshots of the November 14, 1986, Hualien, Taiwan earthquake's mainshock fault plane indicating P wave source locations, including error bars and labeled by rupture times. Uncertainties in rupture times are roughly 2.0 s. See Figure 7.

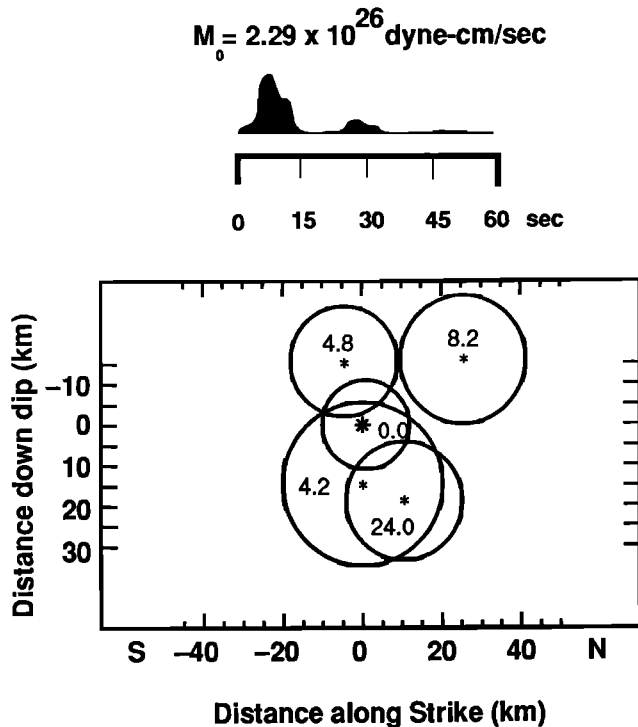$$M_0 = 2.29 \times 10^{26} \text{ dyne-cm/sec}$$

Fig. 12. Teleseismic estimate of the source-time function and the spatial distribution and timing of moment release during the November 14, 1986, Hualien, Taiwan mainshock. The radius of each circle is proportional to the estimated point source seismic moment. Uncertainties in source locations and rupture times were not computed [after *Hwang and Kanamori*, 1989].

event is spread throughout the source volume [*Chen and Wang*, 1988] and shows little correlation with the rupture boundaries. The latter result may be a consequence of a more complicated redistribution of stress after multiple events on different fault planes. We also note that the 1981 event propagated updip, while the 1986 mainshock's direction of propagation is primarily along strike. In contrast, the foreshock of the 1986 event ($M_b = 5.4$) appears to have propagated downdip. These observations are in slight disagreement with the hypothesis that most large earthquakes ($M_L > 5.5$) nucleate at depth and propagate upward [e.g., *Kelleher et al.*, 1973; *Sibson*, 1982; *Das and Scholz*, 1983].

We also note that our analysis has related much of the complexity in the strong ground motion seismograms to spatial and temporal variations in the source. This suggests that detailed predictions of strong ground motion (predictions that include both phase and amplitude information as a function of time) will, in general, require a priori estimates of rupture properties such as spatial variability of slip and rupture velocity. However, we have not related the observed variations in signal strength to strike or dip-slip amplitude and consider it an area for future work.

Additional observations include (1) there are numerous pulses in the strong ground motion seismograms, which are highly correlated across the SMART 1 array, and appear to have been generated

by variations in the source. (2) Hypocenters of events offshore northeastern Taiwan can be determined more accurately using first motion global network data because they are outside the local network. (3) Systematic differences in azimuth between our P and S wave arrivals suggest significant lateral heterogeneity between the sources we studied and the SMART 1 array. *Harris* [1990] has observed similar magnitude refractions in regional phases recorded on a dense array deployed in Kansas. We also note that the November 14, 1986, mainshock appears to have been triggered by a foreshock on an adjacent fault. Our preferred locations and orientations of these faults suggest that the foreshock occurred on a subparallel or splay fault which joins the mainshock fault plane near the end of its rupture zone.

In the previous discussion we argued that our approach provides more detailed observations of rupture propagation than can be obtained using teleseismic methods. We would also like to emphasize that, in contrast to most teleseismic and near-source methods, our approach does not require any assumptions about the spatial and temporal evolution of the source. In spite of these advantages, we are still disappointed by the size of the uncertainties in our source locations and rupture times ($\approx$ 15 km and 3 s). The primary causes of these large uncertainties are the orientations and distances of these faults relative to the array, and the large uncertainties in source parameters and velocity structure. The 1986 event's fault plane dips away from the array at a distance of approximately 80 km, while the 1981 event is oriented nearly edge-on to the array. Simulations indicate that an array sited above the central part of the hanging wall would be much less sensitive to uncertainties in source parameters and velocity structure and could provide much more precise estimates of source locations and rupture times, even if a fairly small number of stations ($\approx$ 10) were used. Based on our simulations and results, we suggest that small dense arrays ($\approx$ 10 stations) sited on land above subduction zones could provide more detailed observations of rupture propagation during large subduction zone earthquakes than has previously been possible. Logical sites include seismic gaps near Ecuador and in the Aleutian Islands [e.g., *Kelleher et al.*, 1973; *Nishenko and Jacob*, 1990].

CONCLUSIONS

We have presented the first direct measurements of two-dimensional rupture propagation. Our measurements include errors which account for uncertainties in hypocentral location, fault plane strike and dip, velocity structure, and slowness estimates. By comparing long-period and high-frequency estimates of duration, we have argued that slip duration was short during the November 14, 1986, Hualien, Taiwan earthquake. Finally, we argue that a dense array would be particularly useful for studying rupture properties of

subduction zone earthquakes and suggest that small ($\approx$ 10 station) dense arrays be sited onshore above seismic gaps which are considered likely to rupture in the near future.

REFERENCES

Abrahamson, N. A., Estimation of seismic wave coherency and rupture velocity using the SMART-1 strong motion array recordings, Ph.D. dissertation, 126 pp., Univ. of Calif., Berkeley, 1985.

Abrahamson, N. A., B. A. Bolt, R. B. Darragh, J. Penzien, and Y. B. Tsai, The SMART 1 accelerograph array (1980-1987): A review, *Earthquake Spectra, 3*, 263-287, 1987.

Angelier, J., Preface to the special issue on: Geodynamics of the Eurasia-Philippine sea plate boundary, *Tectonophysics, 125*, ix-x, 1986.

Archuleta, R. J., A faulting model for the 1979 Imperial Valley earthquake, *J. Geophys. Res., 89*, 4559-4585, 1984.

Benioff, H., Mechanism and strain characteristics of the white wolf fault as indicated by the aftershock sequence, *Calif. Div. Mines Bull., 171*, 199-202, 1955.

Benioff, H., F. Press, and S. Smith, Excitation of the free oscillations of the Earth by earthquakes, *J. Geophys. Res., 66*, 605-619, 1961.

Ben-Menahem, A., and M. Toksoz, Source-mechanism from spectra of long-period seismic surface-waves, 1. The Mongolian earthquake of December 4, 1957, *J. Geophys. Res., 67*, 1943-1955, 1962.

Beroza, G. C., and P. Spudich, Linearized inversion for fault rupture behavior: Application to the 1984, Morgan Hill, California, earthquake, *J. Geophys. Res., 93*, 6275-6296, 1988.

Bolt, B. A., Y. B. Tsai, K. Yeh, and M. K. Hsu, Earthquake strong motions recorded by a large near-source array of digital seismographs, *Earthquake Eng. Structural Dyn., 10*, 561-573, 1982a.

Bolt, B. A., C. H. Loh, J. Penzien, Y. B. Tsai, and Y. T. Yeh, Preliminary report on the SMART 1 strong motion array in Taiwan, Earthquake Engineering Research Center, Berkeley, California, *EERC Rep. UCB/EERC-82/13*, 1982b.

Chen, K. C., and J. H. Wang, A study on aftershocks and focal mechanisms of two 1986 earthquakes in Hualien, Taiwan, *Proc. Geol. Soc. China, 31*, 65-72, 1988.

Darragh, R. B., Analysis of near-source waves: separation of wave types using strong motion array recordings, Ph.D. Dissertation, 144 pp., Univ. of Calif., Berkeley, 1987.

Das, S., and C. H. Scholz, Why large earthquakes do not nucleate at shallow depths, *Nature, 305*, 621-623, 1983.

Goldstein, P., Array measurements of earthquake rupture, Ph.D. dissertation, 191 pp., Univ. of Calif., Santa Barbara, 1988.

Goldstein, P., and R. J. Archuleta, Deterministic frequency-wavenumber methods and direct measurements of rupture

propagation during earthquakes using a dense array: theory and methods, *J. Geophys. Res.*, this issue.

Gutenberg, B., Magnitude determination for larger Kern County shocks, 1952; Effects of station azimuth and calculation methods, *Calif. Div. Mines Bull., 171*, 171-175, 1955.

Hagen, R. A, F. K. Duennebier, and V. Hsu, A seismic refraction study of the crustal structure in the active seismic zone east of Taiwan, *J. Geophys. Res., 93*, 4785-4796, 1988.

Harris, D. B., A comparison of the direction of estimation performance of high-frequency seismic arrays and three-component stations, *Bull. Seismol. Soc. Am., 80*, 1951-1968, 1990.

Hartzell, S. H., and T. H. Heaton, Inversion of strong ground motion and teleseismic waveform data for the fault rupture history of the 1979 Imperial Valley, California, earthquake, *Bull. Seismol. Soc. Am., 73*, 1553-1583, 1983.

Hartzell, S. H., and D. V. Helmburger, Strong-motion modeling of the Imperial Valley earthquake of 1979, *Bull. Seismol. Soc. Am., 72*, 571-596, 1982.

Hwang, L. J., and H. Kanamori, Teleseismic and strong-motion source spectra from two earthquakes in eastern Taiwan, *Bull. Seismol. Soc. Am., 79*, 935-944, 1989.

Kelleher, J., L. Sykes, and J. Oliver, Possible criteria for predicting earthquake locations and their application to major plate boundaries of the Pacific and the Caribbean, *J. Geophys. Res., 78*, 2547-2585, 1973.

Kikuchi, M., and Y. Fukao, Iterative deconvolution of complex body waves from great earthquake—The Tokachi-Oki earthquake of 1968, *Phys. Earth Planet. Inter., 37*, 235-248, 1985.

Mendoza, C., and S. H. Hartzell, Aftershock patterns and mainshock faulting, *Bull. Seismol. Soc. Am., 78*, 1438-1449, 1988.

Niazi, M., Source dynamics of the 1979 Imperial Valley Earthquake from near-source observations of ground acceleration and velocity, *Bull. Seismol. Soc. Am., 72*, 1957-1968, 1982.

Nishenko, S. P., and K. H. Jacob, Seismic potential of the Queen Charlotte-Alaska-Aleutian seismic zone, *J. Geophys. Res., 95*, 2511-2532, 1990.

Olson, A. H., and J. G. Anderson, Implications of frequency domain inversion of earthquake ground motions for resolving the space-time dependence of slip on an extended fault, *Geophys. J. R. Astron. Soc., 94*, 443-455, 1988.

Olson, A. H., and R. J. Apsel, Finite faults and inverse theory with applications to the 1979 Imperial Valley earthquake, *Bull. Seismol. Soc. Am., 72*, 1969-2001, 1982.

Press, F., A. Ben-Menahem, and N. Toksoz, Experimental determination of earthquake fault length and rupture velocity, *J. Geophys. Res., 66*, 3471-3485, 1961.

Roecker, S. W., Y. H. Yeh, and Y. B. Tsai, Three dimensional P and S wave velocity structures beneath Taiwan: Deep structure beneath an arc-continent collision, *J. Geophys. Res., 92*, 10,547-10,570, 1987.

Sibson, R. H., Fault zone models, heat flow, and the depth distribution of earthquakes in the continental crust of the United States, *Bull. Seismol. Soc. Am., 72*, 151-163, 1982.

Spudich, P., and E. Cranswick, Direct observation of rupture propagation during the 1979 Imperial Valley, California, earthquake using a short baseline accelerometer array, *Bull. Seismol. Soc. Am., 74*, 2083-2114, 1984.

Wen, K. L., and Y. T. Yeh, Seismic velocity structure beneath the SMART 1 array, *Bull. Inst. Earth Sci. Acad. Sinica, 4*, 51-72, 1984.

R. J. Archuleta, Department of Geological Sciences, University of California, Santa Barbara, CA 93106

P. Goldstein, Earth Sciences Division, Lawrence Livermore National Laboratory, L-202, P.O. Box 808, Livermore, CA, 94550